Classification Of Large-Scale Environments That Drive The Formation Of Mesoscale Convective Systems Over Southern West Africa

Francis Nkrumah[1,2], Cornelia Klein[3,5], Kwesi Akumenyi Quagraine[1,4], Rebecca Berkoh Oforiwaa[2,6], Nana Ama Browne Klutse[2,6], Patrick Essien[1,2], Gandomè Mayeul Leger Davy Quenum[2,7] and Hubert Azoda Koffi[6]

[1]Department of Physics, University of Cape Coast, Private Mail Bag, Cape Coast, Ghana;
[2]African Institute of Mathematical Sciences (AIMS), Sector Remera, Kigali 20093, Rwanda;
[3]U.K. Centre for Ecology and Hydrology, Wallingford, United Kingdom
[4]Climate System Analysis Group (CSAG), ENGEO, University of Cape Town, Private Bag X3, Rondebosch, Cape Town 7701, South Africa
[5]Department of Atmospheric and Cryospheric Sciences, University of Innsbruck, Innsbruck, Austria
[6]Department of Physics, University of Ghana, Legon P.O. Box LG 63, Ghana
[7]National Institute of Water (NIW), University of Abomey-Calavi, Godomey, Cotonou 01 PB: 4521, Benin

Correspondence to: Francis Nkrumah (francis.nkrumah@ucc.edu.gh) and Nana Ama Browne Klutse (nklutse@ug.edu.gh)

Abstract. Mesoscale convective systems (MCSs) are frequently observed over southern West Africa (SWA) throughout most of the year. These MCS events are the dominating rain-bearing systems, contributing over 50% of annual rainfall over SWA. However, it has not yet been identified what variations in typical large-scale environments of the West African monsoon seasonal cycle may favour MCS occurrence in this region. Here, nine distinct synoptic states are identified and are further associated with being either a dry, transition, or monsoon season synoptic circulation type using self organizing maps (SOMs) with inputs from reanalysis data. We identified a pronounced annual cycle of MCS numbers with frequency peaks in April and October that can be associated with the start of rainfall during the major rainy season and the maximum rainfall for the minor rainy season across SWA respectively. Comparing daily MCS frequencies, MCSs are most likely to develop during transition conditions featuring a northward-displaced moisture anomaly (2.8 MCSs per day), which can be linked to strengthened low-level westerlies. Considering that these transition conditions occur predominantly during the pre- and post-monsoon season, these patterns may in some cases be representative of monsoon onset conditions or a delayed monsoon retreat. On the other hand, under monsoon conditions, we observe weakened low-level south-westerlies during MCS days, which reduce moisture content over the Sahel but introduce more moisture over the coast. Finally, we find a majority of MCS-day synoptic states to exhibit positive zonal wind shear anomalies. Seasons with the strongest zonal wind shear anomalies are associated with the strongest low-level temperature anomalies to the north of SWA, highlighting that a warmer Sahel can promote MCS-favourable conditions in SWA. Overall, the SOMS-identified synoptic states converge towards high moisture and high shear conditions on MCS days in SWA, where the frequency at which these conditions occur depends on the synoptic state.

1 Introduction

The region of West Africa is subject to variability in rainfall on both spatial and temporal scales. Fundamentally, the rainfall pattern in West Africa is modulated by the annual change in the position of the Intertropical Convergence Zone (ITCZ) and the West African Monsoon (WAM). Due to endemic poverty, lack of infrastructure and technology, rapid population increase, and significant fluctuation of the WAM, West Africa has been deemed one of the world's most susceptible regions to climate change (IPCC, 2014). The climate of southern West Africa (SWA) can be categorized into four seasonal stages: a dry season from December to February, two wet seasons lasting from April to June, and September to November, and the so-called little dry season in August (e.g. Thorncroft et al. 2011). Between March and June, when low-level winds are more westerly and the intertropical convergence zone (ITCZ) starts to move northward, the precipitable water peaks over SWA (Klein et al. 2021). The ITCZ retreats southward in September, creating the second rainy season, followed by a dry season from November to January.

One major atmospheric disturbance that contributes to the WAM is the presence of Mesoscale Convective Systems (MCSs) which supplies around 30-80 % of the total rainfall during the WAM (Klein et al. 2018). MCSs are organized thunderstorm clusters, often defined to have a minimum horizontal extent of the precipitating area of 100 kilometres in at least one direction (Guo et al. (2022); Chen et al. (2022); Houze (2004)). Maranan et al. (2018) note that diverse MCS sub-groups such as squall- or disturbance lines, structured convective systems, and mesoscale

57 convective complexes impact the hydro-climate of West Africa. In both the tropics and midlatitudes, MCS also
58 contributes significantly to rainfall extremes, rendering them a substantial contributor to the hydrologic cycle (Feng
59 et al. (2021); Li et al. (2020)). More studies have been motivated in recent decades by evaluating drivers that affect
60 rainfall variability and intensity associated with MCSs (Baidu et al. (2022); Augustin et al. (2022)). MCSs, for
61 instance, supply essential precipitation and, as a result, supply water to agriculturally productive regions in the
62 tropics, particularly in semi-arid regions such as the Sahel (Nesbitt et al. (2006)).

63   However, relative to our understanding of MCS drivers in the Sahel, SWA has received less attention. The
64 connections of MCSs to larger-scale atmospheric motion and states are both important and not fully understood for
65 the southern region, hence, a better understanding of large-scale MCS drivers is important for improving
66 precipitation prediction over SWA. Earlier research has suggested an increasing role of other types of less-organized
67 rainfall in place of MCSs over the Guinea Coast (e.g. (Acheampong, 1982; Fink et al., 2006; Kamara, 1986;
68 Omotosho, 1985), with MCS contribution to annual rainfall decreasing from 71% in the Soudanian to 56% in the
69 coastal zone (Maranan et al 2018), emphasizing MCS importance across the SWA region. Maranan et al., 2018 also
70 concluded that precipitable water and Convective Available Potential Energy (CAPE) determine where MCSs may
71 occur in SWA, while zonal wind shear is a stronger predictor for distinguishing between small scattered convection
72 and MCS-type development. Indeed, zonal wind shear intensification was found to be a major driver of increasing
73 frequencies of the most intense Sahelian MCSs over the last three decades (Taylor et al., 2017), a mechanism that
74 was similarly found to play a role for early-season MCS intensification in SWA (Klein et al 2021). Zonal wind
75 shear, which is thought to modulate the storm-available supply of moist buoyant air, is also seen to be very critical
76 to the organization of convective systems (e.g., Alfaro, 2017; Mohr & Thorncroft, 2006). Accordingly, propagating
77 storms with longer-lasting organized precipitation systems were consistently found to be associated with strong
78 vertical wind shear and higher values of CAPE in the Sahel (Hodges & Thorncroft, 1997; Laing et al., 2008; Mohr
79 & Thorncroft, 2006).

80   Previous studies address the large-scale settings for WAM-related rainfall throughout the seasons (Sultan
81 and Janicot, 2003) with less attention given to the importance of large-scale WAM modes and their effect on
82 regional MCS frequencies in SWA. The role of regional MCS-centred environments in the initiation and
83 development of MCSs in West Africa has been well studied (e.g., Klein et al. 2021; Vizy and Cook 2018; Schrage et
84 al. 2006; Maranan et al. 2018). Vizy and Cook (2018) observed that the extension of vertical mixing to the level of
85 free convection, as a result of surface heating, tends to initiate MCSs in an environment where the mid-tropospheric
86 African easterly wave disturbance is located in the east. The vertical wind shear is enhanced as a result of the
87 synoptic disturbance. Klein et al. (2021) suggested that heavy rainfall, due to cold MCSs during both dry and rainy
88 seasons, occurs in an environment with stronger vertical wind shear, increased low-level humidity, and drier mid-
89 levels. Unlike vertical wind shear, Maranan et al., (2018) suggested that thermodynamic conditions such as CAPE
90 and Convective Inhibition (CIN) are of lesser importance for the horizontal growth of convective systems, although
91 they indicate the potential of the initial vertical development of convective systems. Janiga and Thorncroft (2016)
92 also suggested that CAPE, vertical wind shear and column relative humidity are the decisive large-scale
93 environmental parameters that control the characteristics of convective systems. Based on radar and sounding

94   observations aligned around 15°N, Guy et al. (2011) analyzed MCSs and their respective environmental conditions
95   over three different regimes of West Africa (maritime, coastal, and continental). They concluded that MCSs tend to
96   occur ahead of the African easterly wave (AEW) trough during the maritime and the continental regime, while they
97   are mostly found behind the trough in the coastal regime.

98   It is not clear to what extent different large-scale patterns of atmospheric drivers such as temperature, wind,
99   humidity, and CAPE at different stages of the WAM drive the formation of MCSs over SWA. The SWA region
100   differs from its Sahelian counterpart in its closer proximity to the ocean and a distinct bimodal rainfall seasonality.
101   The WAM stages can broadly be classified into a dry season when north-easterly Harmattan winds prevail over most
102   of West Africa during December-February when rainfall mostly occurs off the southern coast of the continent
103   (Thorncroft et al 2011), and the monsoon season from July-September, initiated by a striking jump of the monsoonal
104   rainfall band from coastal regions to the Sahel (Hagos and Cook, 2007). The monsoon months thus represent the
105   unimodal Sahelian rainfall season. In SWA however, the majority of rainfall occurs between the dry months and
106   monsoon months, when the monsoon rainband first passes northward over southern regions from March to June, and
107   subsequently moves southward again when the monsoon retreats in October (e.g. Maranan et al 2018, Klein et al
108   2021). Here, we define these months when SWA receives most of its rainfall as transition season.

109   From this SWA perspective, our study systematically classifies the different large-scale patterns across the WAM
110   region and how they are associated with MCSs over SWA. For this purpose, a classification using a self organizing
111   map (SOM; Kohonen 2001) analysis was carried out to characterize large-scale WAM patterns during the 1981-
112   2020 period, which we subsequently grouped into days with MCS occurrence over SWA. The SOM is a clustering
113   technique that is topologically sensitive and uses an unsupervised training method to cluster the training data
114   (Lennard and Hegerl, 2014; Quagraine et al. 2019). This methodology thus allows us to identify favourable types of
115   large-scale environments driving the formation of MCSs within different WAM stages.

116   The paper is organized as follows: Section 2 details the study area and data sources and how they were
117   processed. In section 3, the SOM methodology and other needed statistics used to investigate the relationship
118   between large-scale environment patterns and particular MCSs are presented. Section 4 discusses the main results,
119   which include the common features and different types of large-scale patterns associated with MCSs. Section 5
120   provides the summarized conclusions of the study.

121   **2 Data Sources and Processes**

122   **2.1 ERA5 Reanalysis Data and MCS Data**

123   The ECMWF fifth-generation atmospheric reanalysis (Hersbach et al., 2020), ERA5, was used as the main
124   data source in this work. The dataset is generated using 41r2 of the Integrated Forecast System (IFS) model, based
125   on a four-dimensional variational data assimilation scheme, and takes advantage of 137 vertical model levels and a
126   horizontal resolution of 0.28125° (31 km). The data provides hourly estimates of model integration. In this study,
127   hourly zonal and meridional winds (650 and 925 hPa), specific humidity (925 hPa), temperature (925 hPa), and

4   4

128 convective available potential energy (CAPE) in ERA5 during 1981–2020 were used to explore suitable large-scale

129 environments for the development of MCSs in SWA (5-9°N, 10°W-10°E). The zonal and meridional wind at 925

130 hPa, are used to understand the penetration of monsoon flow inland. The zonal wind difference between 925 hPa

131 and 650 hPa is used as a zonal wind shear change indicator while the temperature at 925 hPa is used to visualize

132 Saharan heat low (SHL) differences. Due to the main direction in which MCSs propagate (east to west), enhanced

133 easterly zonal wind shear are presented as positive anomalies as these are positively related to storm development.

134 Specific humidity (q) at 925 hPa was used to explore whether CAPE changes are controlled by low-level q. We

135 consider also the total column water vapour (TCWV) due to its ability to represent the total gaseous water in the

136 vertical column of the atmosphere which is influenced by the evolution of the humidity field. ~~TCWV represents the~~

137 ~~precipitable water the atmosphere holds better than the humidity.~~ The Meteosat Second Generation (MSG)

138 cloud-top temperature data, which are available every 15 minutes from the Eumetsat archives online

139 (https://navigator.eumetsat.int/product/EO:EUM:DAT:MSG:HRSEVIRI) was used in this study. Twelve years of

140 MCS snapshots (2004–15) detected from Meteosat Second Generation 10.8 μm-band brightness temperatures

141 (Schmetz et al., 2002, EUMETSAT 2021) are used to define MCS days in this study. Following (Klein et al., 2021),

142 an MCS is defined here as a -50°C contiguous cloud area larger than 5000 km^2. We consider the MCS images every

143 half hour, for which they are matched up with the half-hourly Integrated Multi-satellite Retrievals for Global

144 Precipitation Measurement (IMERG; Huffman et al. 2019) dataset, using the merged microwave−/−infra-red

145 ("precipitationCal") rainfall product. An "MCS day" is then defined as a day with at least one hour containing 5

146 simultaneously existing MCSs between 16 and 1900 UTC with maximum rainfall >5mm within the SWA domain.

147 Here, only land-based MCSs are considered because MCSs over land are fundamentally more intense and deep than

148 its counterpart over the ocean (Mohr and Zipser 1996).

149

150 **3 Methodology**

151 **3.1 Self-organising Maps (SOMs) analysis**

152 The study uses the self organizing map (SOM; Kohonen 1982, 2001) from SOM-PAK-3.1 software. The

153 technique is used to identify archetype synoptic circulation patterns over the southern West Africa region by training

154 a 9-node SOM with ERA5 daily mean 925 hPa geopotential height fields to produce 9 characteristic circulation

155 patterns for the period 1981 to 2020. The geopotential height circulation pattern is used here mainly based on its

156 physically realistic output spanning a range of circulation features found in the atmosphere (Hewitson and Crane,

157 2002) and its ability to detect the West African Heat Low (WAHL) which is a key element of the West African

158 monsoon system (Lavaysse et al. 2009; Biasutti et al. 2009). The SOM is mostly the preferred choice over other

159 clustering methods such as the principal component analysis (PCA) or K-means because the data is not discretized

160 and orthogonality is not forced or does not require subjective rotations to produce interpretable patterns. The main

161 advantage of the SOM technique is its ability to deal with non-linear data (such as the continuum of atmospheric

162 conditions) and can easily be visualized and interpreted (Reusch et al. 2005; Lennard and Hegerl, 2014). The steps

163 within the technique can be broadly grouped into two stages, namely the training stage and the mapping stage.

164 Earlier studies (e.g. Hewitson and Crane 2002; Kim and Seo 2016; Lee 2017; Rousi et al. 2015; Sheridan and Lee

165 2012) have successfully used this technique in synoptic climatology to effectively preserve relationships between
166 weather states while giving outputs that are readily understood and can be easily visualized as an array of classified
167 patterns. These classified patterns help in interpreting relationships between large-scale regional circulation patterns
168 and local weather expressions and rainfall extremes (Hewitson and Crane 1996; Cassano et al. 2015; Wolski et al.
169 2018). In this study, the SOM is randomly initialized allowing for hidden patterns and structure in the geopotential
170 height at 925 hPa to be discovered while the algorithm iteratively updates the weights of the nodes to better
171 represent the data. The strength of initializing the SOM this way lies also on its robustness to noise and outliers as a
172 result of the algorithm applying a competitive learning structure to the data which then allows for the formation of
173 distinct clusters. The SOM_PAK algorithm allows the SOM process to minimize quantization and topological errors
174 at the mapping stage when choosing the best SOM as outlined in Lennard and Hegerl (2014). However, there is a
175 trade-off when choosing the size of the SOM, as this is dependent on the need to generalize circulation states for
176 analyseis or the need to capture predominant spatial characteristics that affect the local climate. The choice of how
177 many SOM nodes to choose is a trade-off between distinctiveness and robustness. Based on SOM_PAK, we tested
178 node sizes 2x3, 3x3, and 3x4, using the quantization error (QE) as an indicator of the quality and robustness of the
179 respective node size. We find a minimized QE for 3x3 (c.f. Supplementary Figure S1), which, from visual
180 inspection, also shows a larger number of distinct circulation features than 2x3 while producing fewer redundancies
181 than 3x4. Thus, all the following analyses are based on the 3x3 node matrix.

182

183 **3.2 Large-scale WAM patterns on southern West Africa MCS days**

184 Based on the 69 different large-scale node patterns, we explore within-node large-scale conditions that
185 characterize MCS days in SWA. For examination of environmental conditions suitable for SWA MCS activity,
186 large-scale conditions were taken from hourly ERA5 reanalysis data sampled at 1200 UTC when the daily
187 convective activity is more representative of pre-convective atmospheric conditions (Klein et al. 2021). Pre-
188 convective conditions are considered in the study to reduce the effects of feedback from the MCSs on environmental
189 conditions (Song et al. 2019). Composites of ERA5 large-scale environmental variables (temperature, wind, specific
190 humidity, and CAPE) are created for all node days, and for MCS days within each SOM node. Finally, the anomaly
191 in large-scale patterns between MCS days and node mean conditions are computed to determine MCS-favourable
192 adjustments in large-scale patterns within each node. A two-sided Student's t-test is used to determine significant
193 differences between node climatologies and MCS-day sub-samples.

194 In addition to large-scale condition composites, we also sample pre-convective (1200 UTC) local
195 atmospheric conditions (ERA5), for each 1800 UTC MCS at the location of minimum cloud top temperature. We
196 only consider 1800 UTC MCSs for local condition sampling to avoid oversampling similar atmospheric states from
197 several MCS time steps. These conditions are compared to the node climatology conditions at the same locations,
198 allowing us to explore the difference in node climatology versus MCS day conditions at the specific locations where
199 MCSs occurred on respective days. Here we only focus on the afternoon peak of convection when it is triggered and
200 is in early stages of organization. It should be noted that driver importance may shift for nocturnal MCSs in later

201 hours, when CAPE is reduced over night and shear may increase further in importance for MCS maintenance (Vizy
202 et al, 2018)

203 **4 Results**

204 **4.1 Node seasonality and mean conditions**

205   A 9-node SOM (Fig. 1) with distinct synoptic states was identified, where the nodes are hereafter referred
206 to as nodes one (1) to nine (9). Considering the SOM node frequency distributions in Fig. 1, it is noticeable that the
207 nodes separate different stages of the monsoon circulation seasonality, although certain nodes evidently cover a
208 wider range of months that cannot be represented by the typical monthly grouping of the seasonal cycle (e.g.
209 2,3,5,8). Circulation patterns in nodes 1, 4, and 7 can be attributed to cases primarily observed in the first three
210 months (January, February, and March) and the last two months (November, and December), hence a pattern most
211 representative of the dry season months. On the other hand, nodes 2, 5, and 8 depict an environment that is
212 prominent during the pre-monsoon and the post-monsoon seasons, with node 2 presenting a clearer seasonal
213 exclusivity during pre-monsoon while nodes 5 and 8 show frequent occurrences during the post-monsoon season.
214 These nodes (nodes 2, 5, and 8) are hence in the following referred to as transition season nodes, a period that
215 connects the dry and monsoon season. The right-hand side of the SOM nodes 3, 6, and 9 represent patterns that
216 cover monsoon season months, but can similarly feature high frequencies outside of the monsoon season (e.g. node
217 3 with the highest frequency in May).

218
219

220
221

222
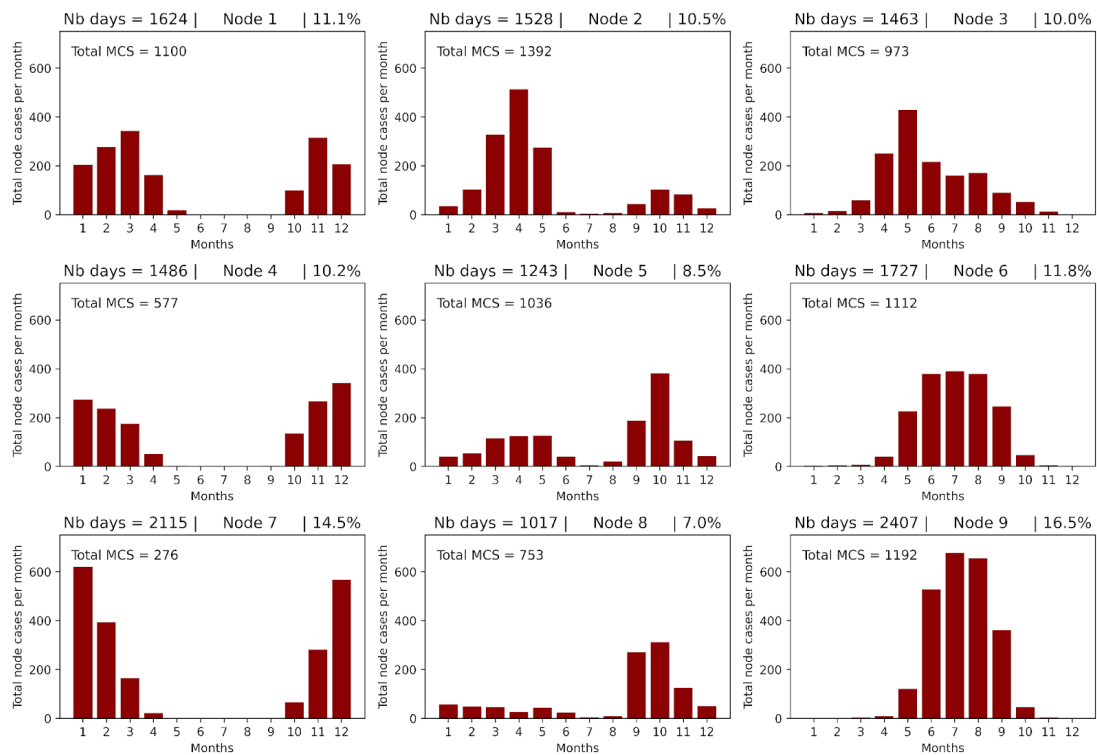
Figure 1. Monthly distribution of node cases based on SOM analysis. Bar values indicate the total number of MCSs per month from 2004 to 2015. The total number of MCS per node from 2004 to 2015 is displayed in node panels. The title shows the total number of days in each node (left) and the contribution of each node to the total node days (right).

227

228

229
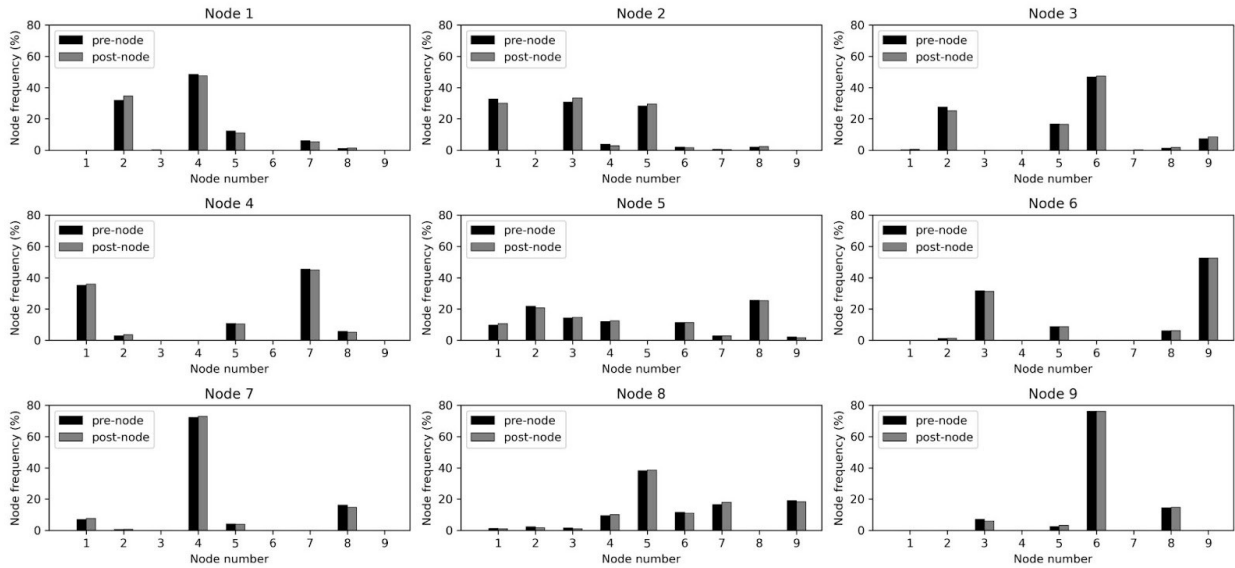
Figure 2: Frequency of nodes (%) preceding (pre-node) or following (post-node) each of the nine nodes.

231

To investigate the relationship between nodes across our 3x3 SOM matrix, we now consider the frequencies at which node states are preceded or followed by other nodes in Fig. 2. The resulting frequency distributions reinforce a classification of the matrix columns into dry (1,4,7), transition (2,5,8) and monsoon (3,6,9) season nodes, with the top row (1,2,3) representing nodes that are preceded or followed by nodes of a different season (column) 20-30% of the time. The bottom row nodes (7,8,9) on the other hand are distinct within-season states that are almost never connected to first row nodes (1,2,3) but are reached via intermediate middle row nodes 4,5,6. The node matrix separates different season states along rows, while columns seem to represent within-season states where upper and lower rows are separate states, temporally connected by conditions captured by middle-row nodes. Finally, the persistence of nodes presented in Fig. 3 reflects the discussed matrix structure, with connecting middle-row nodes 4,5,6 featuring shortest periods with on average 1.7-1.9 days, suggesting more transient states. Nodes 2,9,7 on the other hand show the smallest number of single day occurrences (consecutive node days = 1), pointing towards more stable, persistent conditions with an average period length of 3.8-4.3 days. Regarding node characteristics, it is striking that each seasonal node group features nodes of differing persistence (c.f. node season order for consecutive node days = 1), rendering node persistence a key difference between same-season nodes in the SOM matrix columns.

247

248

249

250
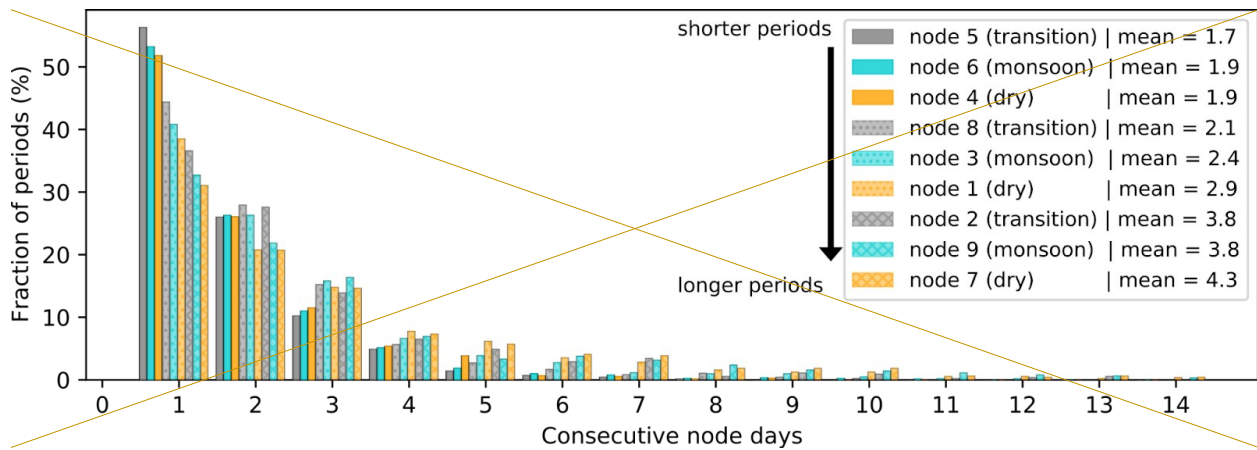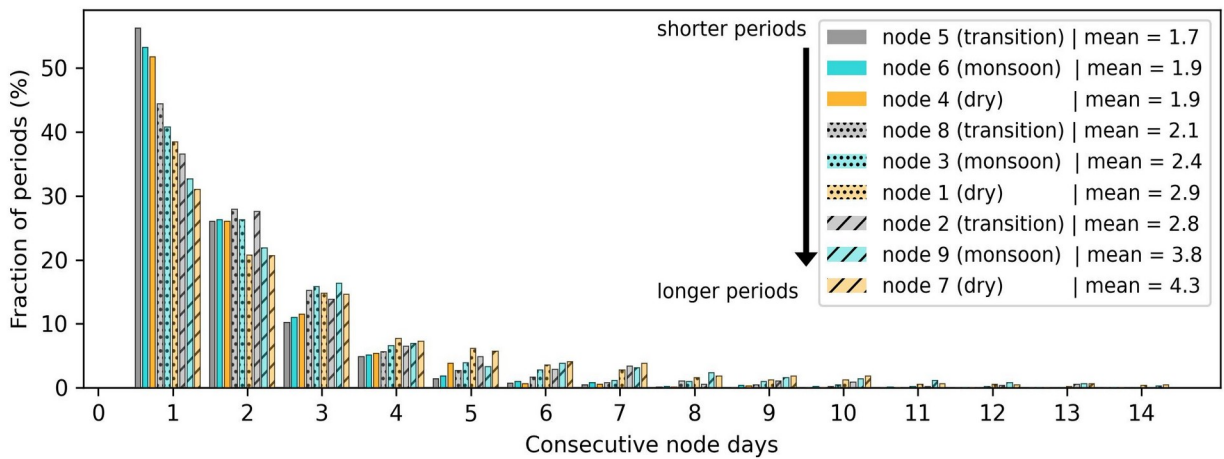
Figure 3: Fraction of periods covering consecutive days of different lengths per node, with the total percentage for 1-14 consecutive node days adding up to 100% per node. The node bars are ordered according to the period fraction for "consecutive node days = 1", revealing the node order going from shorter to longer temporal node persistence, as shown in the legend.

In the following, we inspect the average atmospheric conditions associated with the identified nodes. The SOM classification of different synoptic states was based on 925 hPa geopotential heights, with resulting patterns shown in Fig. 4. The patterns clearly show the signature of the well-known West African Heat Low (e.g. Lavaysse et al. 2009) moving northwards, strengthening over the course of the annual WAM cycle (from nodes 1, 2, and 3) and peaking in August, evident as an area of low pressure over the Sahara in nodes 3, 6, and 9. Nodes 4, 7, and 8 show stages of the weakening of the heat low, coinciding with a southward movement of the 925 hPa low pressure area. The overlaid 650 hPa wind field reveals mean easterly wind conditions at MCS steering levels across all nodes, suggesting that the dominant propagation direction for MCSs remains east to west for all identified synoptic states. As was shown in Fig. 3, the discussed node states have an average duration on the order of days, indicating frequent

transitions. Notably, mid-level westerlies are strengthened or shifted southwards for all top-row nodes in Fig. 4, which is associated with increased probability for MCS occurrence compared to other nodes, as we will outline later (c.f. Fig. 8). Potential synoptic factors that may drive the frequent node transitions and hence affect MCS frequency include extratropical waves, as well as the WAHL that is most pronounced for top-row nodes. WAHL variations were shown to take place on the order of days, in some cases modified by dust concentration (Lavaysse et al. 2011), while its southward expansion on sub-seasonal timescale has been associated with higher shear and more intense MCSs in SWA (e.g. Talib et al. 2022).
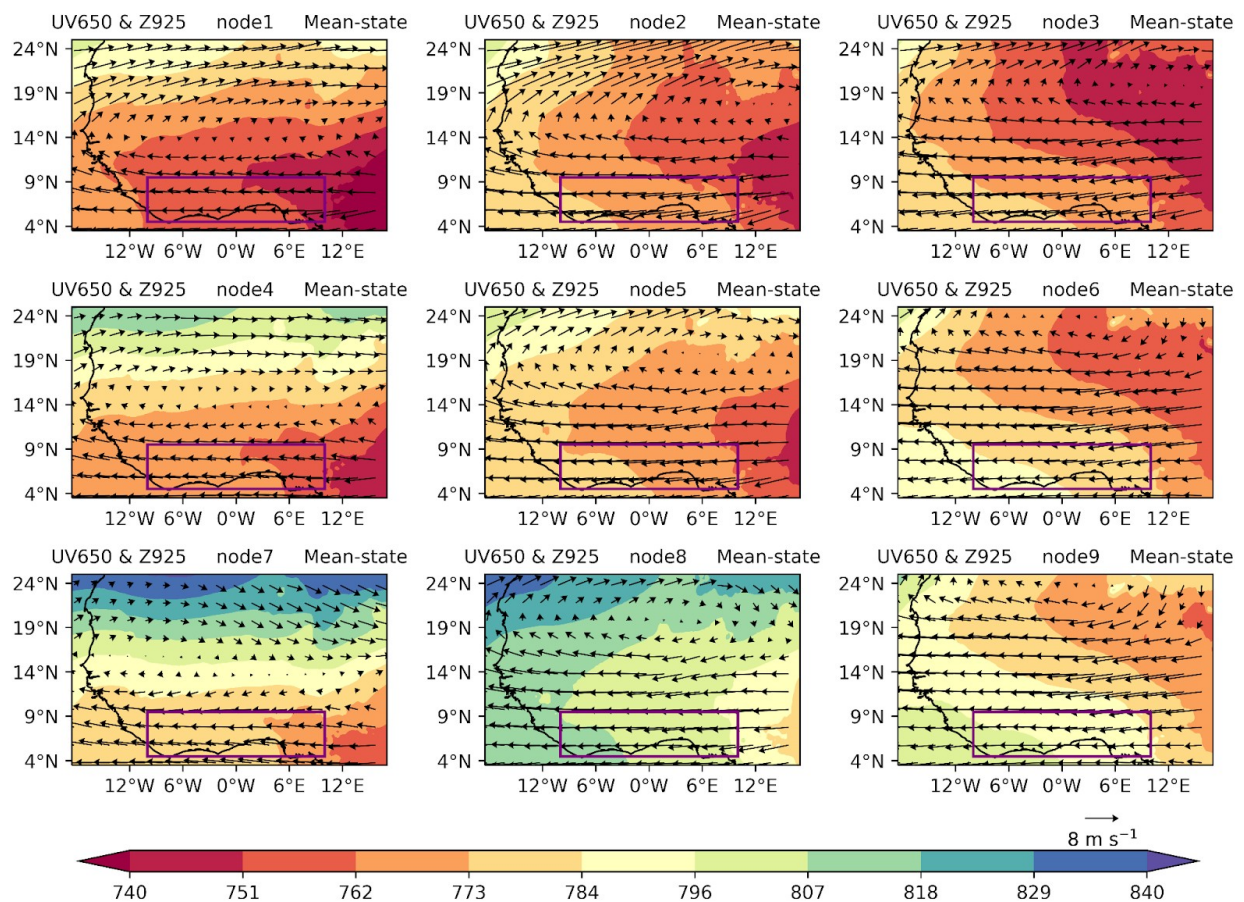
Figure 4. 12 UTC composites of 925-hPa geopotential height (shading; gpm) and 650-hPa winds (vectors; m s^{-1}) in 9 nodes based on SOM analysis. The purple box depicts the SWA region (5º–9ºN, 10ºW–10ºE)

We now examine winds and moisture flows at 925 hPa to explore their behaviour under the nine distinct circulation types identified (Fig. 5). In nodes 1, 4, and 7, the north-easterly winds dominate most of West Africa, with weak southerlies over SWA. This pattern in moisture distribution is evident in the dry season over West Africa,

283 signaling a low moisture presence. The enhanced moisture observed in coastal areas of SWA can be attributed to the
284 penetration of southerly winds. In the transition node 2, the southerly winds strengthen and move inland, causing the
285 north-easterly winds to retreat. A similar effect is observed in nodes 5 and 8 where the north-easterlies become
286 weaker. In nodes 3, 6, and 9, the south-westerlies are intensified and move inland, further enhancing moisture flow
287 from the South Atlantic towards the land, representative of monsoon flow. Wind patterns for mid- and low-levels
288 (Figs. 4 and 5) illustrate vertically-sheared conditions coinciding with regions of high low-level specific humidity in
289 all nodes (purple in Fig. 5), thus marking regions where atmospheric conditions may allow MCS development.

290
291
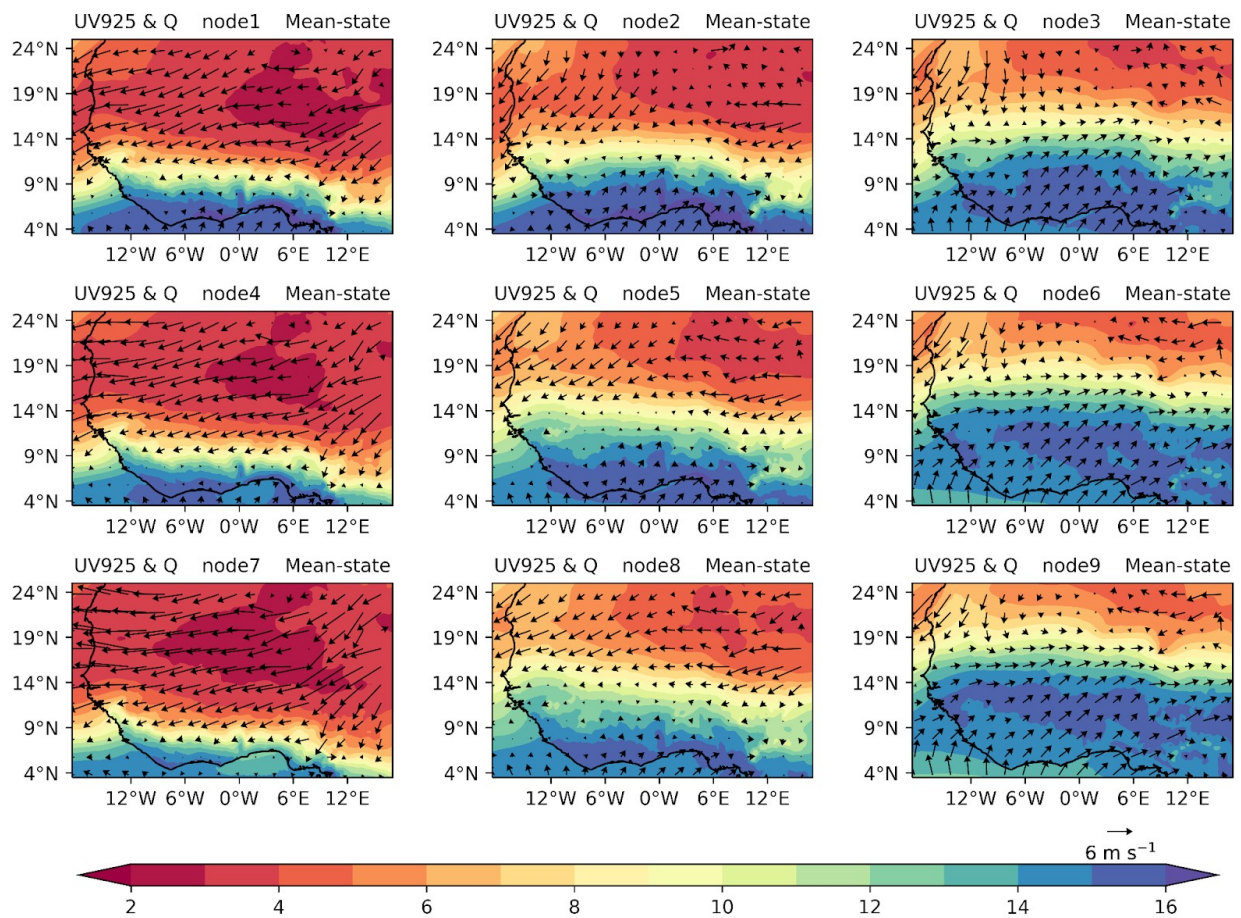
294 **Figure 5.** 12 UTC composites of specific humidity (shading; g kg^{-1}) and 925-hPa winds (vectors; m s^{-1}) in 9 nodes
295 based on SOM analysis.

296

297 A further investigation was conducted to ascertain the spatial distribution of mean zonal wind shear over
298 SWA (Fig. 6), where easterly shear is represented with a positive sign in this study as it is easterly shear that
299 contributes to MCS development in this region. The patterns in zonal wind shear demonstrate northward transport
300 during the propagation of the WAM cycle and a wider spread of zonal wind shear from first to third column nodes

illustrate a strong link of high-shear areas to the propagation of the WAM cycle, and these areas widen as the zonal shear band moves further inland. High-shear areas also closely follow the northern boundary of increased low-level humidity, marking the areas where humidity and shear conditions may allow MCS development. For nodes with high frequency in the monsoon season (nodes 6 and 9), zonal wind shear peaks clearly to the north of the SWA domain. A southward retreat of zonal wind shear is observed during the post-monsoon season (nodes 2, 5, and 8).
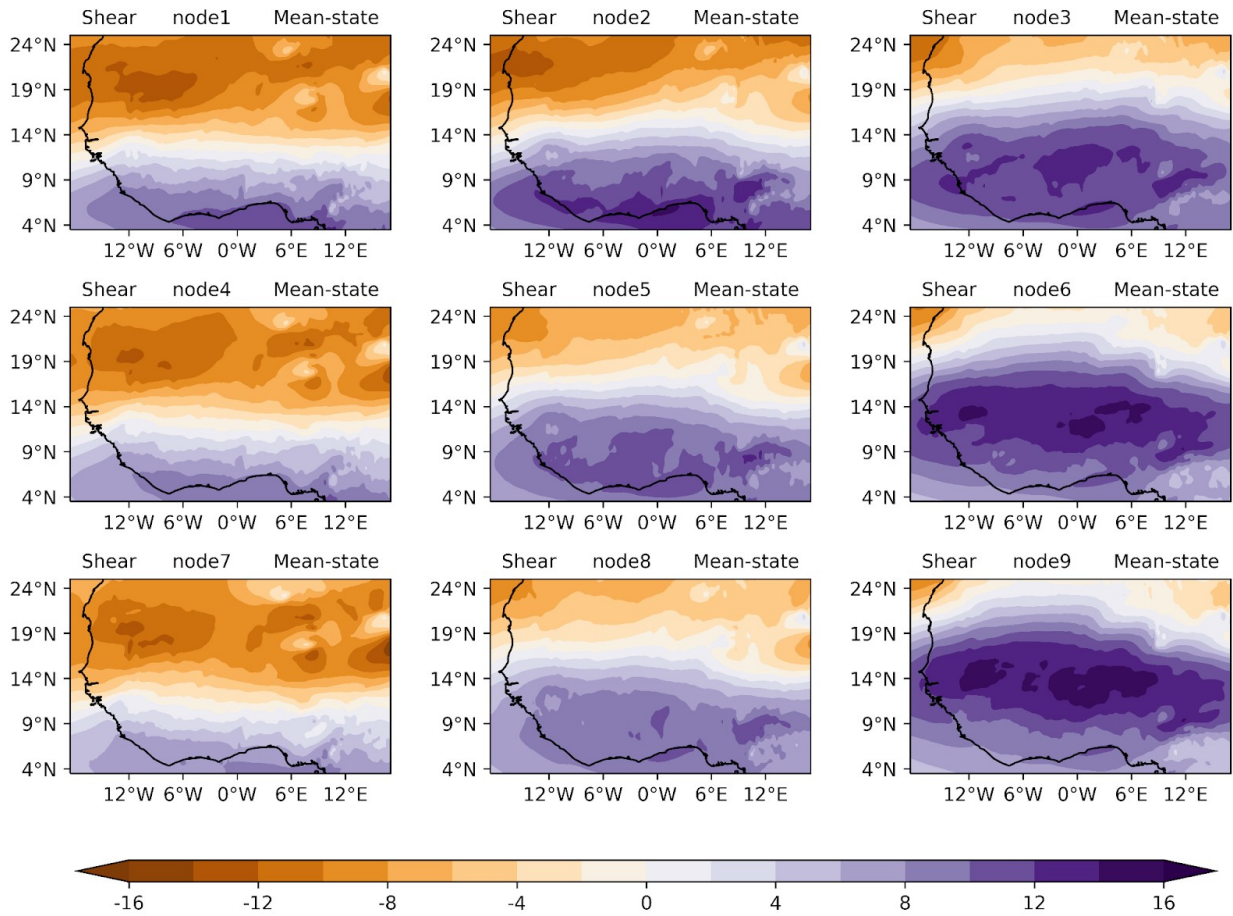
Figure 6. 12 UTC composites of zonal wind shear in 9 nodes based on SOM analysis.

4.2 Large-scale conditions favouring MCS days

The environmental conditions that are associated with MCS occurrence are described in this section. Firstly, the monthly climatology of MCS frequency as captured by our MCS snapshots (average number of MCSs at 1800 UTC across SWA domain) is considered with a focus on rainfall months in Fig. 7, which shows a pronounced annual cycle of MCS numbers with frequency peaks in April and October. These peak months are associated with the start of rainfall during the major rainy season and the maximum rainfall for the minor rainy season across SWA respectively. The monthly climatology of MCS frequency decreases from April to August, with August being the

318 local minimum. This local minimum corresponds to the so-called "little dry season" (Le Barbé et al., 2002; Vollmert
319 et al., 2003) that exists before the southward retreat of the rainbelt.
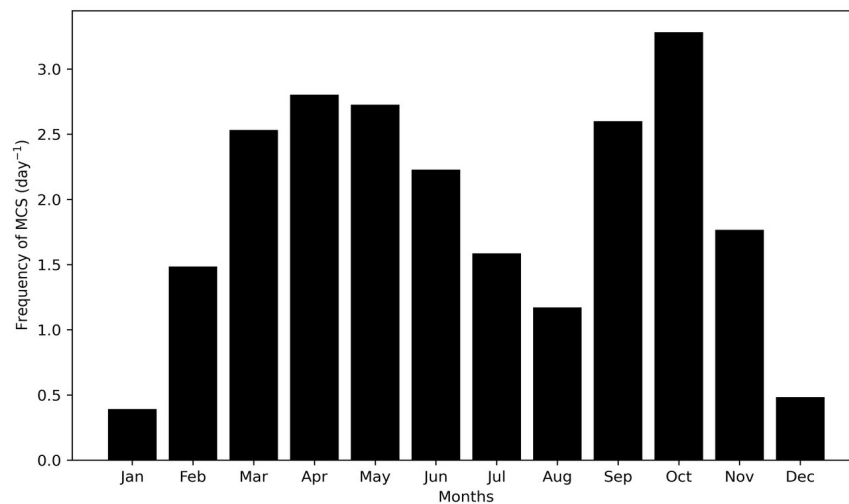
320 **Figure 7.** Average annual cycle of MCSs at 1800 UTC within the SWA box showing the monthly average of MCS
321 number per day.

322

323 The spatial distribution of MCS frequencies during node days is depicted in Fig. 8. Comparing daily MCS
324 frequencies, we find that MCSs are most likely to develop under transition node (2,5,8) conditions (2.8 MCSs per
325 day) featuring a northward-displaced moisture anomaly (Fig. 9). Given the transition nodes occur predominantly
326 during pre-monsoon (late March to June) and post-monsoon (from September to November) - the major and the
327 minor rainy season respectively in SWA (cf. Fig.~1), these patterns may in some cases be representative of early
328 monsoon onset and a delayed monsoon retreat respectively. MCSs ~~more~~ rarely develop under dry node (1,4,7)
329 conditions, with frequencies as low as 0.6 MCSs per day. Frequency signals in node 1 are dominated by land-sea
330 breeze convection along the coast which are gradually suppressed in nodes 4 and 7. Large-scale settings, therefore,
331 seemingly facilitate such rather local-scale developments. Nodes 1 and 9 feature the same overall MCS frequency,
332 where node 1 however shows coastal MCS frequency peaks as is representative for dry season characteristics, while
333 MCS frequency peaks are shifted towards the Sahel during node 9 monsoon conditions.

334

335
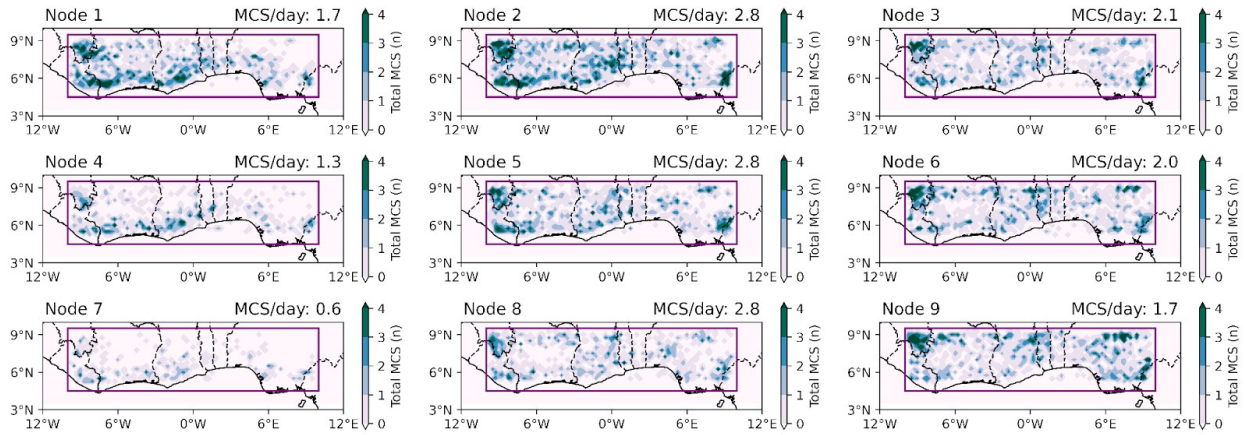
Figure 8. The SWA region indicating the spatial distribution of MCSs during node days. The purple box depicts the main study region of southern West Africa (SWA, 10ºW - 10ºE, 5-9ºN) and titles show the frequency of MCS per day per node within the SWA box.
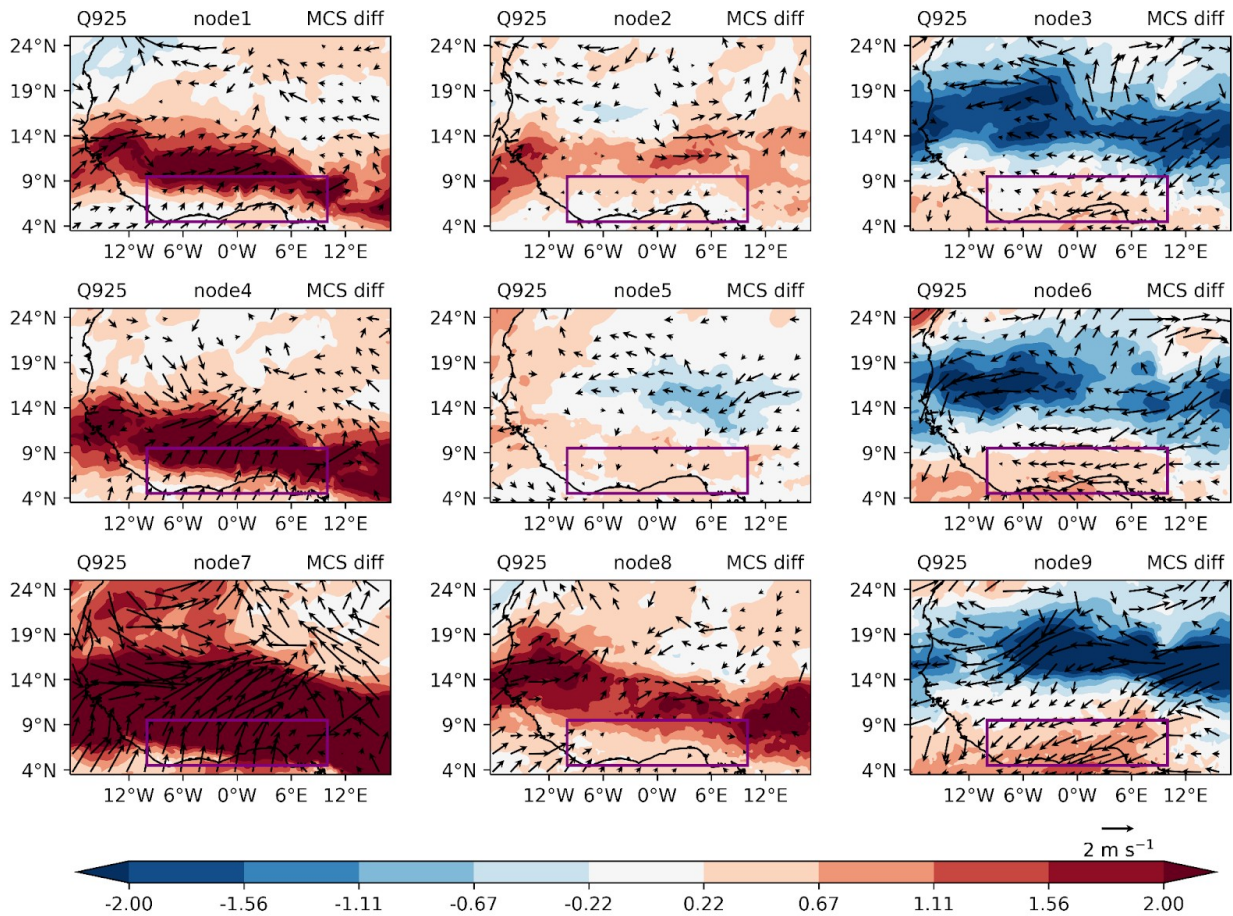
344 **Figure 9.** 12 UTC MCS-day composite anomalies of specific humidity (shading; g kg^{-1}) and 925-hPa winds
345 (vectors; m s^{-1}) in 9 nodes based on SOM analysis. Specific humidity anomalies are shown when they are
346 significant at the 5% level; wind vectors are shown when either the zonal or meridional wind anomalies are
347 significant at the 5% level.
348
349   During the dry season nodes (1,4,7), a positive widespread moisture anomaly maximum is observed with
350 anomalous south-westerly winds over SWA (Fig. 9). This depicts a substantial enhancement in the low-level
351 moisture transport as a result of the few days with convective activities during the dry season. In the transition nodes
352 (2,5,8), low-level moisture anomalies during convective activity days show weak and mostly insignificant behaviour
353 along the SWA coast based on the two-sided Student's t-test. In node 8, a positive moisture anomaly is located over
354 the northern part of SWA. During monsoon nodes (3,6,9), a notable region of anomalous low-level easterly wind is
355 observed over the Sahel, indicating a weakening of the south-westerly monsoon winds and of the low-level westerly
356 jet, which reduces moisture transport towards the Sahel. This is evident in the negative moisture anomalies over the
357 Sahel and the increase in moisture over the coastal regions during MCS days, which can result in less convective
358 activities over the Sahel region and more convective activities over coastal areas.
359   We now consider low-level temperature anomalies to detect potential changes in temperature gradients and
360 SHL strength on MCS days. Figure 10 shows a widespread increase in temperature north of SWA during days with
361 active convection in the dry (1,4,7) and transition (2,8) nodes, which may explain strengthened south-westerly wind
362 anomalies in some of these nodes (c.f. Fig. 9). The SWA region in the dry and transition nodes, on the other hand,
363 reveals a negative and/or insignificant change in temperature during MCS days when compared with the mean
364 climatology. In monsoon nodes 3, 6, and 9, temperatures are enhanced in most parts of West Africa including SWA
365 during days with active convection.
366
367
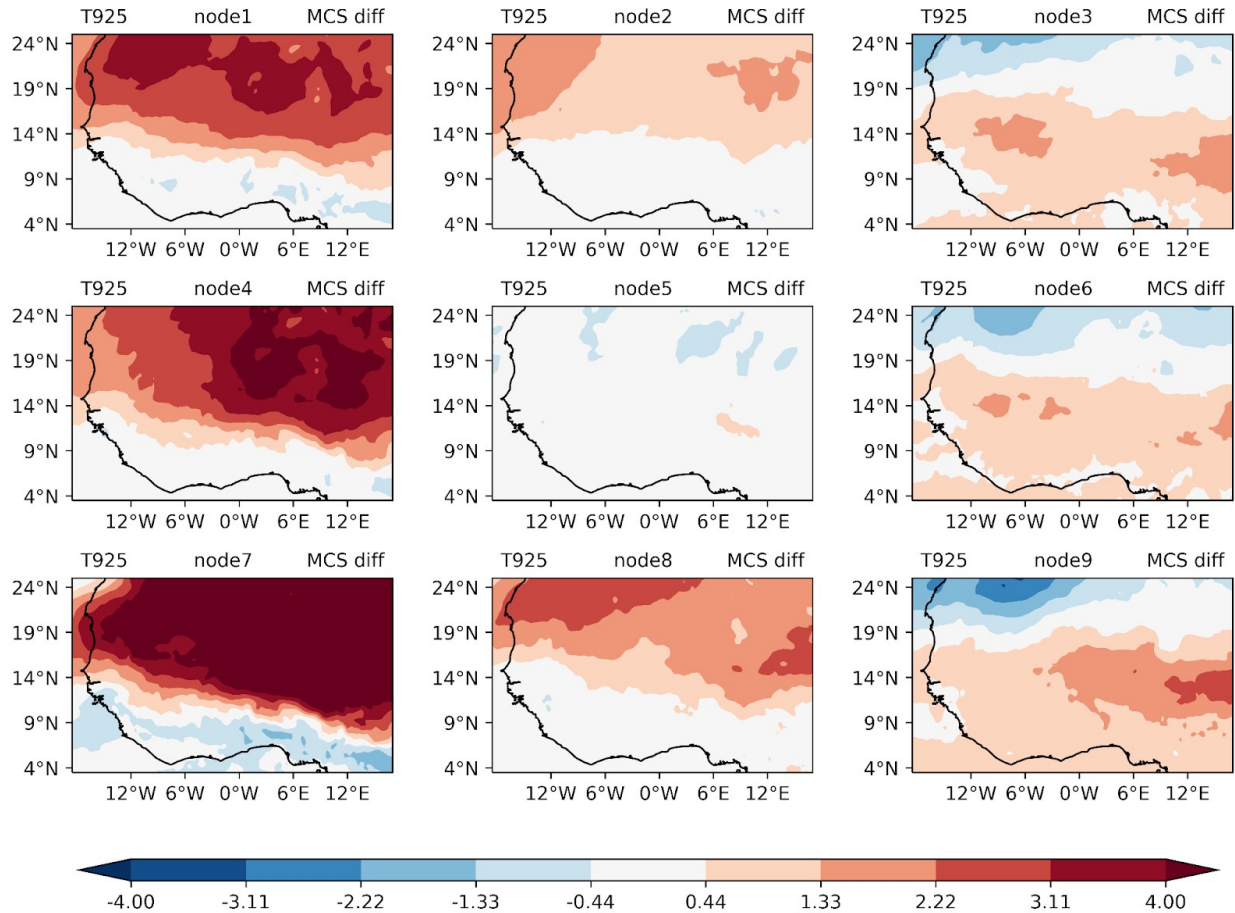
368
369
370 **Figure 10.** 12 UTC composite anomalies of 925hPa temperatures (°C) in 9 nodes based on SOM analysis.
371 Temperature anomalies are shown when they are significant at the 5% level.

372

373   Figure 11 shows the spatial distribution of zonal wind shear anomaly between days with convective MCSs
374 over SWA and the climatological zonal wind shear mean for the 9 different nodes across West Africa. Generally, all
375 dry and transition nodes except node 5, reveal a widespread increase in easterly zonal wind shear anomaly over
376 West Africa with the dry nodes depicting stronger events. Zonal wind shear anomalies tend to be stronger and
377 easterly during the dry –season with their peak partly over SWA, but resides to the north of SWA during the
378 transition seasons (nodes 2 and 8). –The positive shear anomaly patterns align with patterns of strengthened
379 temperature gradients for respective dry and transition season nodes (c.f. Fig. 10): only node 5 shows no large-scale
380 temperature anomalies and consequently patchy changes in shear, while strongest shear increases occur for node 7
381 alongside the highest temperature gradient increase. Nodes 2 and 8 experience an appreciably significant increase in
382 easterly zonal wind shear over SWA for MCS days during the transition seasons. The monsoon nodes (3,6,9), on the
383 other hand, exhibit a significant increase in easterly zonal wind shear mainly confined to the south with a
384 pronounced signal in node 9 associated with a peak in eastern-Sahel warming (Fig. 10). In line with the expected
385 zonal wind shear response to an increased large-scale meridional temperature gradient, we thus find the strongest

386 easterly zonal wind shear anomalies for nodes with strongest positive low-level temperature anomalies to the north

387 of SWA (nodes 1,4,7; followed by nodes 2,8), highlighting that a warmer Sahel can promote MCS-favourable shear

388 conditions in SWA.

389

390
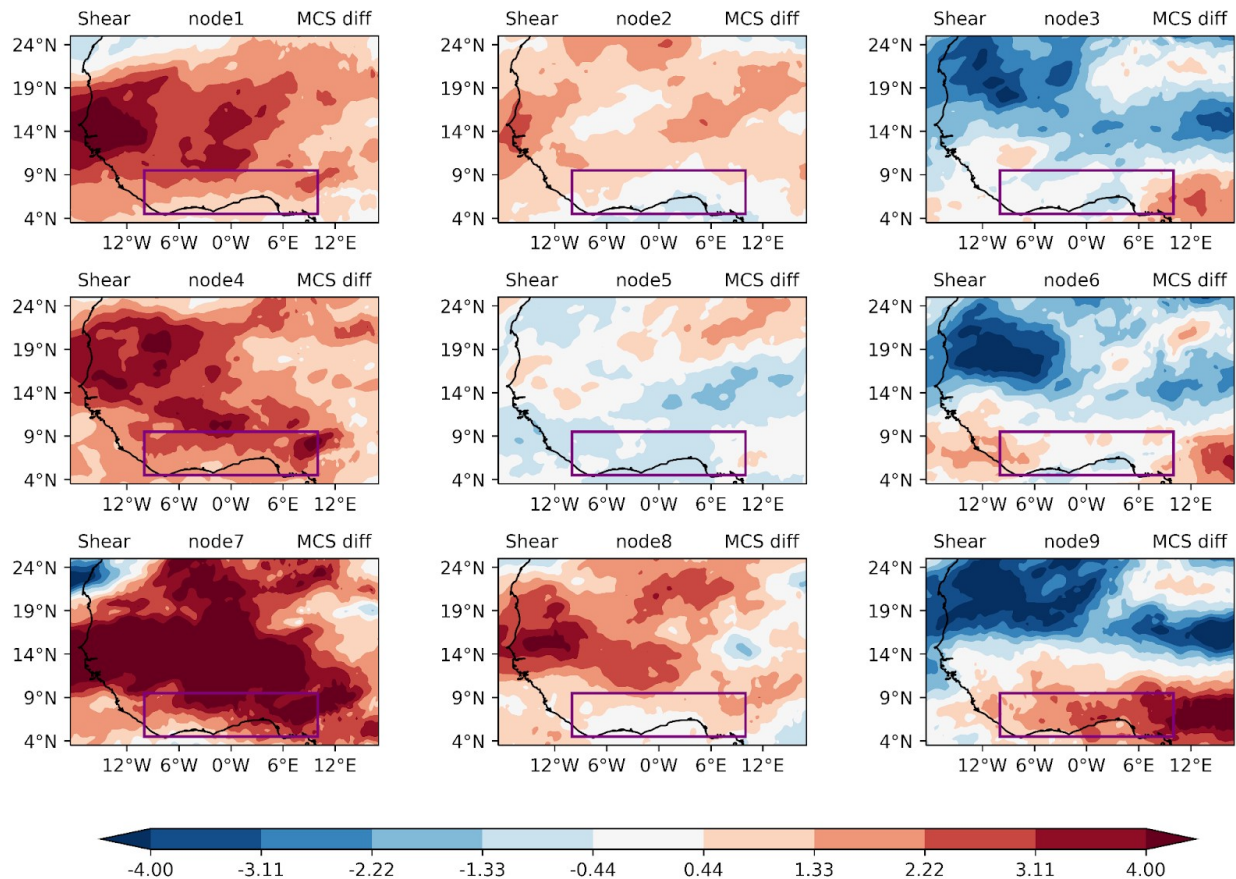
391

392 **Figure 11.** 12 UTC composite anomalies of zonal wind shear (m s⁻¹) in 9 nodes based on SOM analysis. zonal wind

393 shear anomalies are shown when they are significant at the 5% level.

394

395   Investigating the first-order condition for convection development, we also evaluate CAPE for a parcel at

396 925 hPa to ascertain the level of increased MCS-day instability in various nodes over SWA (Fig. 12). A large strip

397 of higher CAPE values extending over the entire region of SWA and the southern Sahel from 5°N−15°N is observed

398 (dry and transition nodes). This large strip of higher CAPE is situated mainly in central and east of SWA, while part

399 of the west coast tends to depict patterns of lower CAPE values, suggesting increased MCS likelihood only for the

400 central and eastern parts of the domain. During monsoon nodes, node 3 shows a ~~swath~~broad strip of high CAPE

401 values in particular to the coast and in some instances extends to the entire SWA (node 6) and north of SWA (node

402 9). Higher CAPE conditions over SWA are to differing degrees significantly associated with decreased CAPE in the

403 Sahelian region, creating a dipole pattern that can occur during transition and monsoon periods according to node

404 frequencies (cf. Fig 1). Overall, all nodes show positive CAPE and negative convective inhibition (c.f.

405 Supplementary Fig. S4) anomalies for MCS days in parts of SWA, creating an environment sufficiently unstable to

406 support the development of convection. The close alignment with regions of increased low-level humidity (Fig. 9)

407 suggests increased low-level moisture advection as the main driver for these instability changes.

408
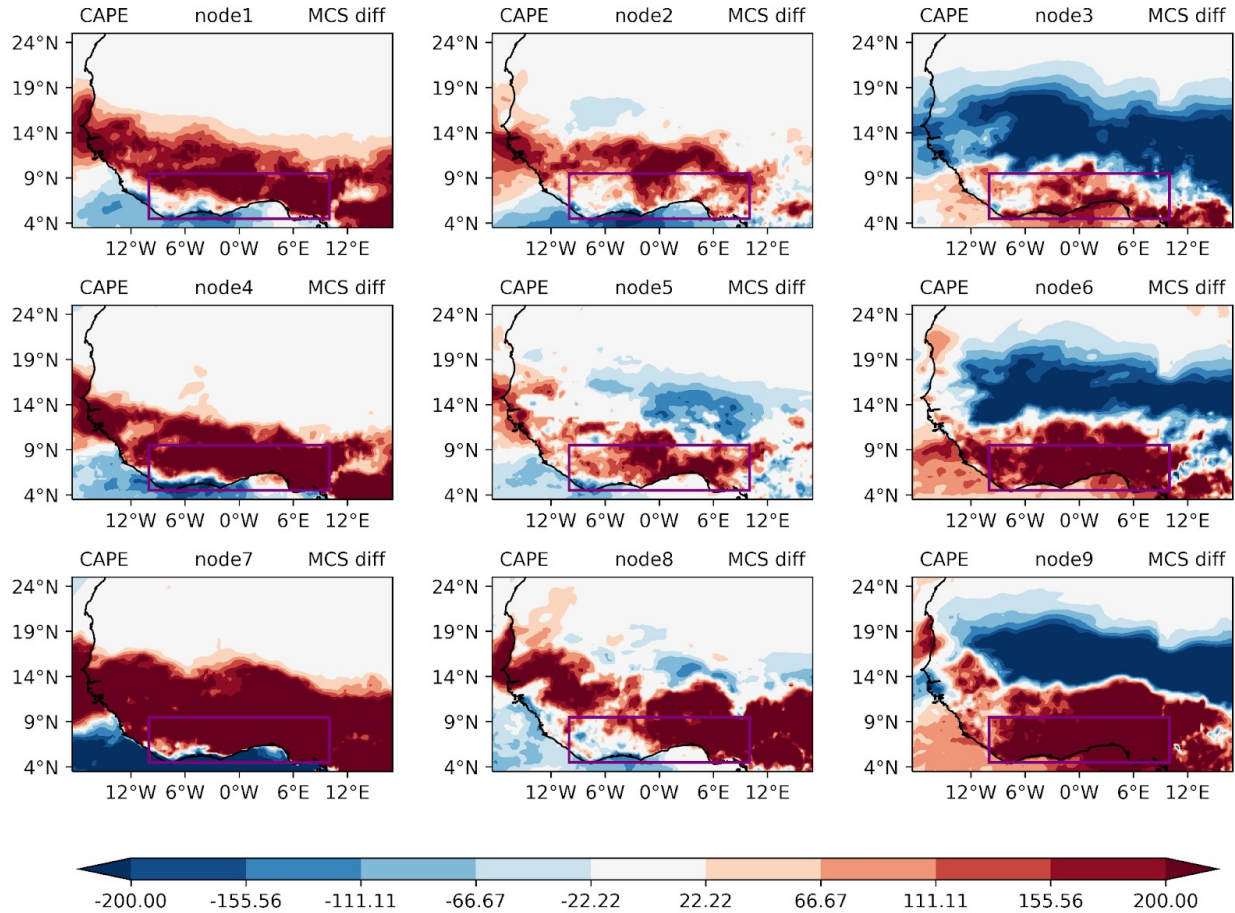
Figure 12. 12 UTC composite anomalies of CAPE (J kg^{-1}) for MCSs occurring in each type of large-scale environment determined by the SOM analysis over SWA. CAPE anomalies are shown when they are significant at the 5% level.

413

4.3 MCS driver variability within nodes

415   The drivers of MCSs within different nodes are considered to examine their relative importance within the

416 different large-scale states (Fig. 13), concentrating on total column water vapor (TCWV) and zonal wind shear.

417 TCWV instead of single-level specific humidity is used here to capture the changes in total moisture available to

418 MCSs under the different regimes. For this analysis, both atmospheric drivers were sampled locally under pre-

419 convective conditions at 1200 UTC at the location where MCSs occurred subsequently at 1800 UTC. Dry season

420 nodes (1,4,7) exhibit the lowest climatological conditions in both wind shear and TCWV. This illustrates the

421 relatively hostile conditions for storms in the mean for these nodes, predominantly representing dry season

422 conditions and explaining the low storm frequency of only 0.6-1.7 MCSs per day (cf. Fig. 9). All monsoon nodes

423   (3,6,9) show on average slightly higher TCWV than transition nodes (2,5,8), but covering a similar range of shear

424   conditions. Considering MCS day conditions, most nodes feature significantly higher TCWV and shear conditions

425   relative to the climatological mean node states. Solely for monsoon season nodes (3,6,9), TCWV shows no

426   significant change, while shear still increases for nodes 6 and 9. Note that while monsoon months feature higher

427   TCWV and similar shear conditions compared to transition nodes for MCS-location climatologies in Fig. 13, a

428   larger domain area is affected by MCS-favourable conditions for transition nodes (c.f. Figs. 5,6). As a consequence,

429   transition nodes exhibit higher overall MCS frequencies. Interestingly, for MCS days, dry season node conditions

430   even move into the ranges of climatological conditions identified for transition season nodes, though still exhibit the

431   lowest values in TCWV and zonal wind shear compared to MCS day conditions of transition and monsoon season

432   nodes.
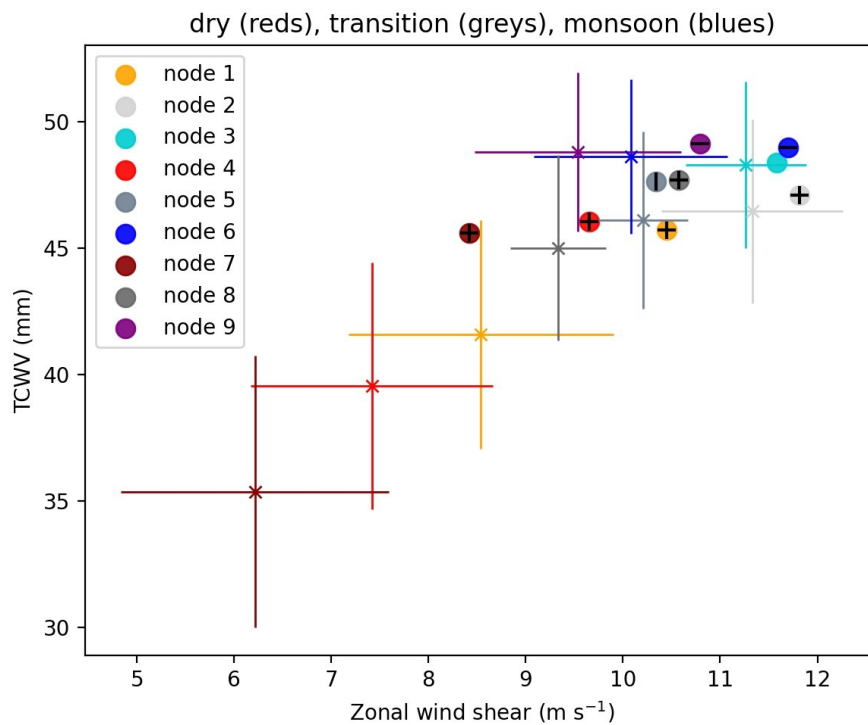
451   **Figure 13.** Mean node climatologies and MCS-day conditions over SWA. The node climatologies are depicted as

452   (x) with whiskers extending one standard deviation. Circles denote corresponding mean MCS-day conditions.

453   Horizontal black lines in the circles indicate significant differences in the shear mean, while a vertical black line

454   marks a significant difference in the TCWV mean against node climatologies based on Welch's t-tests (p < 0.05)

457   Generally, it can be noted that all nodes show increased TCWV on MCS days compared to their

458   climatology. The smallest changes for both TCWV and zonal wind shear between climatology and MCS day occur

459   for node 3, which has its highest frequency for pre-monsoon transition month May but is still common throughout

19   19

460 the monsoon season– (c.f. Fig. 1)–. Together with node 5, it is also the only node for which zonal wind shear

461 conditions remain approximately similar, but with climatological zonal wind shear strengths already reaching > 10

462 m/s at MCS location. Overall, mean node environmental conditions become more similar for MCS-days relative to

463 the climatologies, illustrating that favourable MCS conditions converge towards high TCWV and high zonal wind

464 shear environments irrespective of the large-scale situation.

5 Conclusion

In this study, we identified nine synoptic states over West Africa and examined what changes are associated with favourable MCS environments in Southern West Africa under these states. For the definition of synoptic states and MCS days, we used self-organizing maps (SOM) based on ERA5 925 hPa geopotential height data and 12 years of MCS imagery using Meteosat Second Generation (MSG) 10.8 μm-band brightness temperature data (2004-15), respectively. To investigate how the distinct synoptic states change to support MCS development in SWA, we compared mean climatological node states to node sub-samples of MCS days in SWA. We found the identified synoptic states, based on a 3x3 SOM matrix, to exhibit frequency distributions that are linked to different phases of the West African seasonal rainfall cycle, which we classified as dry (nodes 1, 4, 7), transition (nodes 2, 5, 8) and monsoon (nodes 3, 6, 9) season, albeit most nodes are not strictly confined to one season. We found that different nodes identified within one season exhibit key differences in persistence (consecutive node days) and node succession. Specifically, each season (dry, transition, monsoon) contains a node that is frequently preceded or followed by a node of another season (nodes 1, 2, 3), as well as a node that predominantly shows within-season succession (nodes 7, 8, 9). The shortest node persistence of 1.7-1.9 days was found for nodes 4, 5, and 6. These nodes at the same time represent intermediate synoptic states that develop from or into a different node of the same season. The SOM methodology thus seems a promising approach to identify states of variability beyond the established West African monsoon phases (e.g. Thorncroft et al 2011).

In spite of these clear differences in node persistence and succession, large-scale differences in node climatologies of atmospheric MCS drivers (low-level wind field, 925hPa humidity, and temperature, CAPE) are most pronounced between nodes of different seasons, while same-season nodes show strong pattern similarities. Notably, however, MCS-day node anomalies, as compared to full node climatologies, all show clear increases in low-level humidity and/or wind shear over the SWA region, which are important ingredients for MCS development (Klein et al. 2021). For dry season nodes, these changes are associated with higher temperatures in the Sahel and Sahara, driving stronger south-westerly humid winds inland while increasing shear due to an enhanced meridional temperature gradient on land. Monsoon season nodes on the other hand show the opposite, where a weakening of the south-westerlies and of the Sahelian low-level westerly jet indicates a south-ward shift of the monsoon circulation. This results in more moisture, and for nodes 6, 9 also in higher shear, over SWA, where the latter is linked to a warmer and presumably drier Sahel during monsoonal southward shifts, creating a dipole pattern. Generally, we find the strongest MCS-day zonal wind shear anomalies over SWA for nodes with the strongest low-level temperature anomalies to the north of SWA, representative of favorable MCS conditions in SWA during periods of a warmer

495 Sahel. Strengthened wind shear due to a warmer Sahara was previously also identified to drive MCS intensification
496 in the Sahel (Taylor et al. 2017).

497 Thus, meridional displacements of the extent to which south-westerly winds from the Atlantic penetrate
498 inland and the associated positioning of the meridional temperature gradient seems to be key mechanisms by which
499 MCS days in SWA are created for both, dry and monsoon season node synoptic states. Such meridional
500 displacements have previously been identified as important drivers of monsoon variability on inter-annual (e.g.
501 Nicholson and Webster 2008) and intra-seasonal (e.g. Janicot et al. 2011, Talib et al. 2022) timescales. Here, we are
502 looking at higher-frequency changes with average node persistence between 1.7-4.3 days. Transition nodes show
503 weaker signals and a mixture of a southward (node 5) or northward (node 8) displaced circulation, which may be
504 linked to the fact that these nodes predominantly occur in months when the monsoon circulation and its rainfall band
505 are positioned over SWA (Maranan et al. 2018). Indeed, we find MCSs to be most likely to develop under transition
506 season node conditions (2.8 MCS/day across SWA domain). There is strong potential for further exploration of the
507 synoptic differences between transition season nodes and their meridional shifts on MCS days, as these may in some
508 cases be representative of monsoon onset conditions or a delayed monsoon retreat.

509 Pre-convective atmospheric anomalies at locations where afternoon development of MCSs took place were
510 found to be weakest for transition season node 5, lacking significant changes in wind shear, and for monsoon season
511 nodes 3, 6, 9, for which none showed significant changes in total column moisture, albeit increased moisture at low-
512 levels contributes to elevated CAPE. Here it should be noted that weak anomalies signify nodes whose mean
513 climatological conditions already tend to be more favorable for MCS development with respect to that variable, such
514 that MCS days differ little from the node mean, which, perhaps expectedly, is the case for certain transition and
515 monsoon rather than dry season nodes.

516 Generally, however, we find node environmental conditions to become more similar for MCS days relative
517 to their node climatologies, illustrating that favorable MCS conditions converge towards high TCWV/high zonal
518 wind shear states. Overall, our results show that MCSs develop on average in high moisture, high zonal wind shear
519 local environments under all large-scale situations throughout the year. The large-scale situation however defines the
520 frequency at which favorable MCS environments can occur.

521

522 *Code and data availability*. Codes for the findings of this study are available upon reasonable request from the
523 authors. The processing of ERA5 data made direct access to the primary data archive held at ECMWF, and is
524 available from the Copernicus Data Store (https://cds.climate.copernicus.eu/) and the MSG data are available from
525 http://www.eumetsat.int.

526

527 *Author contributions*. FN, NABK and CK conceptualized the study, with input from KAQ; All authors contributed
528 to and discussed the methodological design, and analyses were conducted by FN and CK; FN, ROB and KAQ wrote
529 the manuscript draft; CK, NABK, PE, GMLDQ and HAK reviewed and edited the manuscript.

530

531 *Competing interests*. The contact author has declared that none of the authors has any competing interests.

Acknowledgments. This work is supported by a grant from the Government of Canada, provided through Global Affairs Canada, www.international.gc.ca (accessed on 1 January 2021), and the International Development Research Centre, www.idrc.ca, (accessed on 1 June 2022) to the African Institute for Mathematical Sciences—Next Einstein Initiative (AIMS-NEI) [Number: 108246-001]. CK acknowledges funding from the NERC-funded LMCS project (NE/W001888/1). KQ also acknowledges funding from the National Research Foundation (NRF), South Africa.

References

Alfaro, D. A.: Low-Tropospheric Shear in the Structure of Squall Lines: Impacts on Latent Heating under Layer-Lifting Ascent, J Atmos Sci., 74, 229–48, https://doi.org/10.1175/JAS-D-16-0168.1, 2017.

Augustin, D., Pascal, I.M., Jores, T.K., Elisabeth, F.D., Cesar, M.B., Michael, T.F., Roméo-Ledoux, D.T., Marceline, M., Gladys, K.N.F. and Firmin, B.A.: Impact Assessment of the West African Monsoon on Convective Precipitations over the Far North Region of Cameroon, Adv. Space Res., https://doi.org/10.1016/j.asr.2022.04.044, 2022.

Baidu, M., Schwendike, J., Marsham, J.H. and Bain, C.: Effects of Vertical Wind Shear on Intensities of Mesoscale Convective Systems over West and Central Africa, Atmos. Sci. Lett, e1094, https://doi.org/10.1002/asl.1094, 2022.

Biasutti, M., Sobel, A. H., & Camargo, S. J.: The role of the Sahara low in summertime Sahel rainfall variability and change in the CMIP3 models. Journal of Climate, 22(21), 5755-5771, https://doi.org/10.1175/2009JCLI2969.1, 2009.

Cassano, E.N., Glisan, J.M., Cassano, J.J., Gutowski Jr, W.J. and Seefeldt, M.W.: Self-Organizing Map Analysis of Widespread Temperature Extremes in Alaska and Canada, Clim. Res. 62, 199-218, https://doi.org/10.3354/cr01274, 2015.

Chen, Y., Luo, Y. and Liu, B.: General Features and Synoptic-Scale Environments of Mesoscale Convective Systems over South China during the 2013-2017 Pre-Summer Rainy Seasons, Atmos. Res.*,* 266, https://doi.org/10.1016/j.atmosres.2021.105954, 2022.

Feng, Z., Leung, L.R., Liu, N., Wang, J., Houze Jr, R.A., Li, J., Hardin, J.C., Chen, D. and Guo, J. A.: Global High-Resolution Mesoscale Convective System Database Using Satellite-Derived Cloud Tops, Surface Precipitation, and Tracking, J. Geophys. Res. Atmos. 126, e2020JD034202, https://doi.org/10.1029/2020JD034202, 2021.

Guo, Y., Du, Y., Lu, R., Feng, X., Li, J., Zhang, Y. and Mai, Z.: The Characteristics of Mesoscale Convective Systems Generated over the Yunnan-Guizhou Plateau during the Warm Seasons, Int. J. Climatol., http://doi.org/10.1002/joc.7647, 2022.

Guy, N., Rutledge, S.A. and Cifelli, R.: "Radar Characteristics of Continental, Coastal, and Maritime Convection Observed during AMMA/NAMMA", Q. J. R. Meteorol. Soc. 137, 1241-56, http://doi.org/10.1002/qj.839, 2011.

Hagos, S. M. and Cook, K. H.: Dynamics of the West African Monsoon Jump, J. Clim., 20(21), 5264–5284, https://doi:10.1175/2007JCLI1533.1, 2007.

Hewitson, B. C., & Crane, R. G.: Climate Downscaling: Techniques and Application. Clim. Res. 7, 85-95, https://doi.org/10.3354/cr007085, 1996.

570 Hewitson, B. C., & Crane, R. G. "Self-Organizing Maps: Applications to Synoptic Climatology." Clim. Res. 22, 13-
571   26, https://doi:10.3354/cr022013, 2002.

572 Hodges, K.I. and Thorncroft, C.D.: Distribution and Statistics of African Mesoscale Convective Weather Systems
573   Based on the ISCCP Meteosat Imagery, Mon Weather Rev 125, 2821-37, https://doi.org/10.1175/1520-
574   0493(1997)125<2821:DASOAM>2.0.CO;2, 1997.

575 Houze Jr, Robert A.: Mesoscale Convective Systems", Rev. Geophys., 42, http://doi:10.1029/ 2004RG000150,
576   2004.

577   Hussain, M.S., Kim, S. and Lee, S.: On the Relationship between Indian Ocean Dipole Events and the Precipitation
578   of Pakistan, Theor. Appl. Climatol. 130, 673-85, http://doi.org/10.1007/s00704-016-1902-y, 2017.

579 IPCC: Climate Change, 2014: Synthesis Report. Contribution of Working groups I, II, and III to the Fifth
580   Assessment Report of the Intergovernmental Panel on Climate Change [Core Working Team, R.K. Pachauri
581   and L.A. Meyer (eds)]. IPCC, Geneva, Switzerland, 151, 2014

582 Janicot, S., Caniaux, G., Chauvin, F., De Coëtlogon, G., Fontaine, B., Hall, N., Kiladis, G., Lafore, J.-P., Lavaysse,
583   C., Lavender, S.L., Leroux, S., Marteau, R., Mounier, F., Philippon, N., Roehrig, R., Sultan, B. and Taylor,
584   C.M.: Intraseasonal variability of the West African monsoon. Atmospheric Science Letters, 12, 58–66,
585   https://doi.org/10.1002/asl.280, 2011

586 Janiga, M.A. and Thorncroft, C.D.: The Influence of African Easterly Waves on Convection over Tropical Africa
587   and the East Atlantic, Mon Weather Rev 144, 171-92, https://doi.org/10.1175/MWR-D-14-00419.1, 2016.

588 Kamara, S. I.: The Origins and Types of Rainfall in West Africa, Weather 41, 48-56, https://doi.org/10.1002/j.1477-
589   8696.1986.tb03787.x, 1986.

590 Kim, H.K. and Seo, K.H.: Cluster Analysis of Tropical Cyclone Tracks over the Western North Pacific Using a Self-
591   Organizing Map, JCLI 29, 3731-51, https://doi.org/10.1175/JCLI-D-15-0380.1, 2016.

592 Klein, C., Belušić, D., & Taylor, C. M.: Wavelet scale analysis of mesoscale convective systems for detecting deep
593   convection from infrared imagery.Journal of Geophysical Research: Atmospheres, 123, 3035 - 3050.
594   https://doi.org/10.1002/2017JD027432, 2018.

595 Klein, C., Nkrumah, F., Taylor, C.M. and Adefisan, E.A.: Seasonality and Trends of Drivers of Mesoscale
596   Convective Systems in Southern West Africa, JCLI 34, 71-87, https://doi.org/10.1175/JCLI-D-20-0194.1,
597   2021.

598 Kohonen, T. "Self-Organizing Maps.-Springer Series in Information Sciences, V. 30, Springer Sci. Rev.,
599   https://doi.org/10.1007/978-3-642-56927-2, 2001.

600 Kusangaya, S., Warburton, M.L., Van Garderen, E.A. and Jewitt, G.P.: Impacts of Climate Change on Water
601   Resources in Southern Africa: A Review, Phys. Chem. Earth., 47-54,
602   https://doi.org/10.1016/j.pce.2013.09.014, 2014.

603 Laing, A.G., Carbone, R., Levizzani, V. and Tuttle, J.: The Propagation and Diurnal Cycles of Deep Convection in
604   Northern Tropical Africa, Q J R Meteorol Soc. 134, 93-109, http://doi.org/10.1002/qj.194, 2008.

605 Lavaysse, C., Flamant, C., Janicot, S., Parker, D.J., Lafore, J.P., Sultan, B. and Pelon, J.: Seasonal Evolution of the
606   West African Heat Low: A Climatological Perspective, Clim. Dyn. 33, 313-30,
607   https://doi.org/10.1007/s00382-009-0553-4, 2009.

Lavaysse, C., Chaboureau, J.-P. and Flamant, C.: Dust impact on the West African heat low in summertime. Q.J.R. Meteorol. Soc., 137: 1227-1240. https://doi.org/10.1002/qj.844, 2011.

Le Barbé, L., Lebel, T., & Tapsoba, D.: Rainfall variability in West Africa during the years 1950 - 90. J. Clim. 15(2), 187-202, https://doi.org/10.1175/1520-0442(2002)015<0187:RVIWAD>2.0. CO;2, 2002.

Li, P., Moseley, C., Prein, A.F., Chen, H., Li, J., Furtado, K. and Zhou, T.: Mesoscale Convective System Precipitation Characteristics over East Asia. Part I: Regional Differences and Seasonal Variations, J. Clim. 33, 9271-86, https://doi.org/10.1175/JCLI-D-20-0072.1, 2020.

Maranan, M., Fink, A.H. and Knippertz, P.: Rainfall Types over Southern West Africa: Objective Identification, Climatology and Synoptic Environment, Q J R Meteorol Soc. 144, 1628-48, https://doi.org/10.1002/qj.3345, 2018.

Mohr, K. I., and Zipser, E. J.: Mesoscale convective systems defined by their 85-GHz ice scattering signature: Size and intensity comparison over tropical oceans and continents. *Mon. Wea. Rev.*, 124, 2417-2437, https://doi:10.1175/1520-0493(1996)124<2417:MCSDBT>2.0.CO;2, 1996

Mohr, K.I. and Thorncroft, C.D.: Intense Convective Systems in West Africa and Their Relationship to the African Easterly Jet, Q J R Meteorol Soc. 132, 163-76, https://doi.org/10.1256/qj.05.55, 2006.

Nesbitt, S.W., Cifelli, R. and Rutledge, S.A.: Storm Morphology and Rainfall Characteristics of TRMM Precipitation Features, Mon Weather Rev 134, 2702-21, https://doi.org/10.1175/MWR3200.1, 2006.

Nicholson, S. E. and Webster, P. J.: A physical basis for the interannual variability of rainfall in the Sahel, Q. J. R. Meteorol. Soc., 2084 (November), 2065–2084, doi:10.1002/qj, 2008.

Queralt, S., Hernández, E., Barriopedro, D., Gallego, D., Ribera, P. and Casanova, C.: North Atlantic Oscillation Influence and Weather Types Associated with Winter Total and Extreme Precipitation Events in Spain, Atmos. Res. 94, 675-83, https://doi.org/10.1016/j.atmosres.2009. 09.005, 2009.

Schmetz, J., Pili, P., Tjemkes, S., Just, D., Kerkmann, J., Rota, S. and Ratier, A.: An Introduction to Meteosat Second Generation (MSG)", Bull Am Meteorol Soc 83, 977-92, https://doi.org/10.1175/1520-0477(2002)083<0977:AITMSG>2.3.CO;2, 2002.

Schrage, J.M., Fink, A.H., Ermert, V. and Ahlonsou, E.D.: Three MCS Cases Occurring in Different Synoptic Environments in the Sub-Sahelian Wet Zone during the 2002 West African Monsoon, J Atmos Sci 63, 2369-82, https://doi.org/10.1175/JAS3757.1, 2006.

Sheridan, S. and Lee, C.C.: Synoptic Climatology and the Analysis of Atmospheric Teleconnections, Prog Phys Geogr. 36, 548-57, https://doi/org/10.1177/0309133312447935, 2012.

Sultan, B., & Janicot, S.: The West African monsoon dynamics. Part II: The "preonset" and "onset" of the summer monsoon. Journal of climate, 16(21), 3407-3427, https://doi.org/10.1175/1520-0442(2003)016<3407:TWAMDP>2.0.CO;2, 2003.

Talib, J., Taylor, C. M., Klein, C., Harris, B. L., Anderson, S. R. and Semeena, V. S.: The sensitivity of the West African monsoon circulation to intraseasonal soil moisture feedbacks, Q. J. R. Meteorol. Soc., 148(745), 1709–1730, doi:10.1002/qj.4274, 2022.

Taylor, C.M., Belušić, D., Guichard, F., Parker, D.J., Vischel, T., Bock, O., Harris, P.P., Janicot, S., Klein, C. and Panthou, G.: Frequency of Extreme Sahelian Storms Tripled since 1982 in Satellite Observations, Nature 544, 475-78, https://doi.org/10.1038/nature22069, 2017.

647 Thorncroft, C. D., Nguyen, H., Zhang, C. and Peyrille, P.: Annual cycle of the West African monsoon: Regional
648   circulations and associated water vapour transport, Q. J. R. Meteorol. Soc., 137(654), 129–147,
649   https://doi:10.1002/qj.728, 2011.

650 Vizy, E.K. and Cook, K.H.: Mesoscale Convective Systems and Nocturnal Rainfall over the West African Sahel:
651   Role of the Inter-Tropical Front, Clim. Dyn. 50, 587-614, https://doi.org/10.1007/s00382-009-0553-4, 2018.

652 Wolski, P., Jack, C., Tadross, M., van Aardenne, L. and Lennard, C.: Interannual Rainfall Variability and SOM-
653   Based Circulation Classification", Clim. Dyn. 50, 479-92, https://doi/org/10.1007/s00382 -017-3621-1, 2018.
654